ACS SENSORS

pubs.acs.org/acssensors

Article

Programmable Y-Shaped Probes with Proximity Bivalent Recognition for Rapid Electrochemiluminescence Response of Acute Myocardial Infarction

Xian-Ming Guo, Mei-Ling Zhao, Wen-Bin Liang, Xia Yang, Ruo Yuan, and Ying Zhuo*

Cite This: *ACS Sens.* 2022, 7, 3208−3215

Read Online

ACCESS | Metrics & More | Article Recommendations | Supporting Information

ABSTRACT: Herein, an exogenous luminophore-free and disposable electrochemiluminescence (ECL) biosensor was established for rapid response of acute myocardial infarction (AMI) using programmable Y-shaped probes (Y-probes) with proximity bivalent recognition. Specifically, the indium tin oxide thin film coated glass electrode (ITO) was modified with urchin-like porous TiO_2 microspheres ($pTiO_2$ MSs), which could achieve strong and stable ECL in $S_2O_8^{2-}$ solution due to the dual promoting effect of the coreaction accelerator $pTiO_2$ MSs, exhibiting 2.7-fold higher ECL intensity in comparison with that of bare ITO. Moreover, the Y-probes as bivalent recognition elements containing two kinds of cardiac troponin I (cTnI, a biomarker of AMI) aptamers and a linker labeled with ferrocene (L-Fc) were designed to export a "signal off" mode. When the target cTnI was in the proximity of the Y-probes, the L-Fc was separated from the electrode surface due to the proximity recognition of cTnI and its aptamers, achieving the highly effective recovery of ECL, which allowed for a much more rapid detection of cTnI than the sandwich-type immunoassay. As a proof of concept, an exogenous luminophore-free and disposable ECL platform for rapid and sensitive monitoring of cTnI was obtained and displayed a desired linear range from 100 fg mL^{-1} to 100 ng mL^{-1} with a limit of detection (LOD) of 30.1 fg mL^{-1}, which can be ingeniously expanded as a portable home tester with ECL biosensors developments.

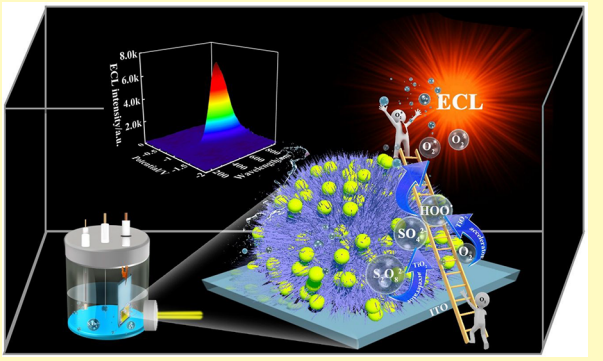

KEYWORDS: *exogenous luminophore-free, electrochemiluminescence biosensor, Y-shaped DNA probes, proximity recognition, cTnI*

The sensitive and accurate detection of cardiac troponin I (cTnI) is critical for acute myocardial infarction (AMI), the content of which is considered to be the "gold standard" for acute AMI diagnosis.[1] At present, sandwich-type immunoassays are widely used for the detection of cTnI due to their sensitivity and precision.[2] However, multiple incubation steps and washing cycles were needed in their workflows, which was time-consuming and labor-intensive. Moreover, an antibody as a protein probe could be easily affected by environmental factors such as pH, temperature, or salt concentration. Compared with antibody−antigen recognition, the employment of aptamers as recognition elements provides a number of benefits, including high thermal stability, strong binding affinity, economic cost, and easy operation.[3] To improve the identification efficiency, proximity probes were developed with two recognition sites in close space, enabling a dramatic increase of the local effective concentration and binding affinity of the affinity probes.[4] Inspired by these backgrounds, the programmable Y-shaped DNA proximity probes (Y-probes) as bivalent recognition elements containing two kinds of cTnI aptamers with different recognition sites were designed, thus allowing for highly specific recognition and rapid detection of cTnI.

Electrochemiluminescence (ECL), combined with the advantages of electrochemistry and luminescence analysis, has become one of the most important bioanalytical methods in vitro with its high sensitivity,[5] low background,[6,7] and high controllability.[8−10] Conventionally, the $S_2O_8^{2-}$ is one of the most widely used coreaction reagents in most cathode ECL process, such as ruthenium complexes,[11,12] polycyclic aromatic hydrocarbons,[13] and quantum dots,[14−16] because it has the characteristics of chemical stability and moderate electrochemical reactivity. Recent research demonstrated the ECL signal could also be generated from excited mode of singlet oxygen ($^1(O_2)_2$*) in $S_2O_8^{2-}$ solution, which is produced by the free radical reaction of reactive oxide species (ROS) and $SO_4^{\bullet-}$ from electrochemical reduction process of dissolved oxygen (DO) and $S_2O_8^{2-}$, respectively. However, on account of the

Received: August 22, 2022
Accepted: October 4, 2022
Published: October 14, 2022

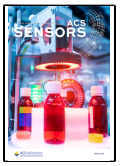

Scheme 1. (A) Schematic Diagram of the Fabrication of the Y-Probes and the Operational Principle of the cTnI Biosensor. (B) ECL Reaction Mechanism of Biosensor with the "Signal off/on" Mode

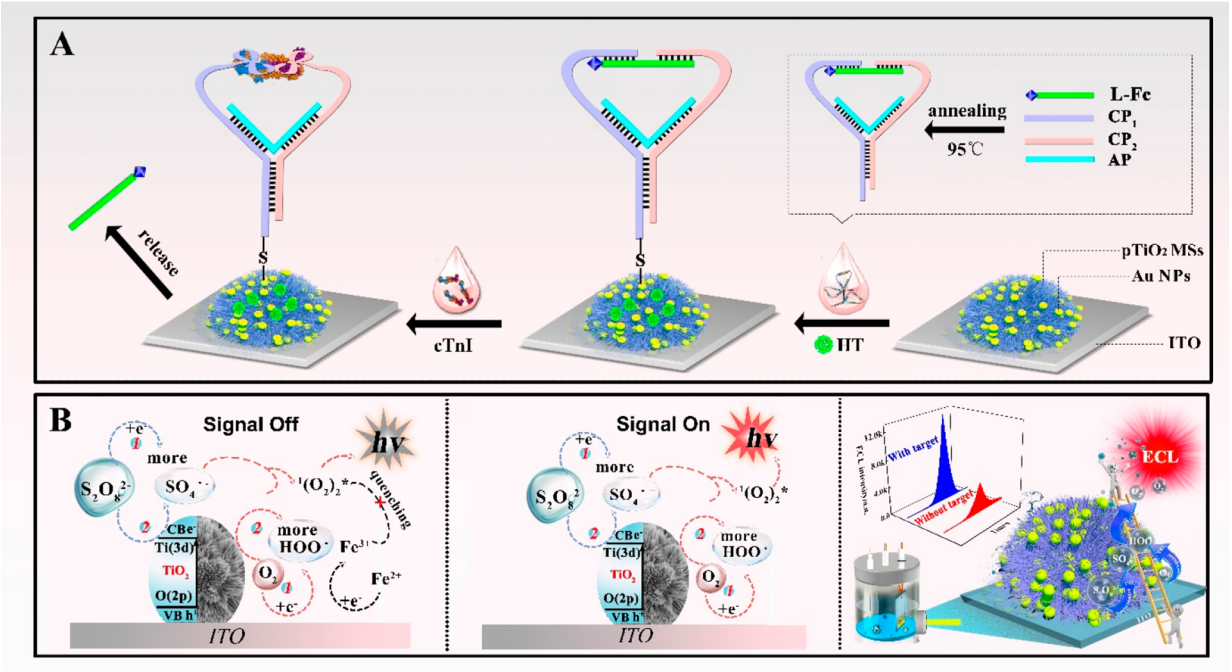

low reactivity of DO, it is hard to provide an available ECL platform for the practical application of bioanalysis. With the development of the ECL ternary system in previous work,[17,18] the reaction efficiency of $S_2O_8^{2-}$ was significantly improved with the employment of the coreaction accelerators, which could promote the $S_2O_8^{2-}$ to increase the yield of $SO_4^{\bullet-}$. Notably, TiO_2 nanomaterials with unique photoelectric properties and long-term chemical stability are widely used as interface material in the construction of biosensors. Han's group[19] reported that TiO_2 nanoparticles, a coreaction accelerator, could boost the electrochemical reduction efficiency of coreactant $S_2O_8^{2-}$ at the cathode, enhancing the ECL emission of Zr metal organic framework (PCN-224). Recently, TiO_2 nanoflowers were developed to catalyze DO to generate the strong oxidizing radical ROS, which significantly amplified the ECL of Ag nanoclusters as the coreaction accelerator.[20] Thus, the TiO_2 nanomaterials have the potential to display the dual promoting effect toward the redox of both $S_2O_8^{2-}$ and DO. In addition, indium tin oxide thin film coated glass (ITO), as the most common disposable electrode, is usually used to construct electrochemical devices. With this motivation, a sea urchin-like porous TiO_2 microspheres ($pTiO_2$ MSs) modified ITO ($pTiO_2$ MSs/ITO) was developed as a disposable and low-cost ECL sensing interface. It was surprising to find that the extremely stronger and more stable ECL emission was achieved on the $pTiO_2$ MSs/ITO without any exogenous luminophores in the $S_2O_8^{2-}$ solution in comparison with that of the bare ITO, which has rarely been reported yet.

Taking advantage of the remarkable ECL intensity of $pTiO_2$ MSs/ITO, a disposable, rapid and low-cost cTnI biosensor was established through a highly specific Y-shaped bivalent recognition element with proximal binding interaction. As depicted in Scheme 1A, capture probes (CP1 and CP2), assistant probe (AP), and a linker labeled with ferrocene (L-Fc) were hybridized with each other to form Y-probes, which were immobilized on the Au NPs/$pTiO_2$ MSs/ITO via the Au−S covalent bond, achieving an extraordinarily low ECL signal ("signal off" mode) due to the presence of Fc molecules. Prior to this process, the $pTiO_2$ MSs were coated on the bare ITO surface to form a homogeneous film, which provided a strong and stable ECL signal in $S_2O_8^{2-}$ solution, attributed to the dual promoting effect. To prove the feasibility of the concept, the Y-probes were applied to construct an ECL switch platform for the detection of cTnI. When the targets have approached the bonding sites of Y-probes, the L-Fc was released from the sensing interface, accompanying with a recovery of ECL response ("signal on" state). The ECL reaction mechanism of biosensor with the "signal off/on" mode was depicted in Scheme 1B, which was described in detail in the Results and Discussion. Such a new strategy integrating sensing interface ($pTiO_2$ MSs/ITO) with Y-probes may be ingeniously expanded as a portable home tester in the foreseeable future.

EXPERIMENTAL SECTION

Reagents, apparatus, fabrication of biosensor, ECL measurement procedure and gel electrophoresis are described in Sections 1−5 of Supporting Information (SI).

$pTiO_2$ MSs Preparation. The solvothermal method was used to synthesize the $pTiO_2$ MSs.[21] First, 0.35 g hexadecyl trimethylammonium bromide (CTAB) and 50 mL deionized water were mixed together followed by sequential addition of 1 mL titanium tetraisopropanol (TTIP) and 1 mL concentrated HCl (35%) into the resultant solution to form a transparent gel by vigorous swirling at 25 °C for 1 h. Then, 25 mL of the aforementioned gel was mixed with 25 mL ethylene glycol and 0.3 g urea and stirred until a homogeneous mixture formed. After that, a 50 mL Teflon vessel was used to transfer the obtained mixture and kept inside for 20 h at 150 °C. Eventually, the precipitates were alternately washed with phosphate buffered saline (PBS) and ethanol until the washing solution became colorless, and dried at 80 °C for 24 h for future usage.

Y-probe Preparation. To make the well-designed Y-probes (1 μM), a combination of equal volume of the DNA strands CP_1 (4

https://doi.org/10.1021/acssensors.2c01832
ACS Sens. 2022, 7, 3208−3215

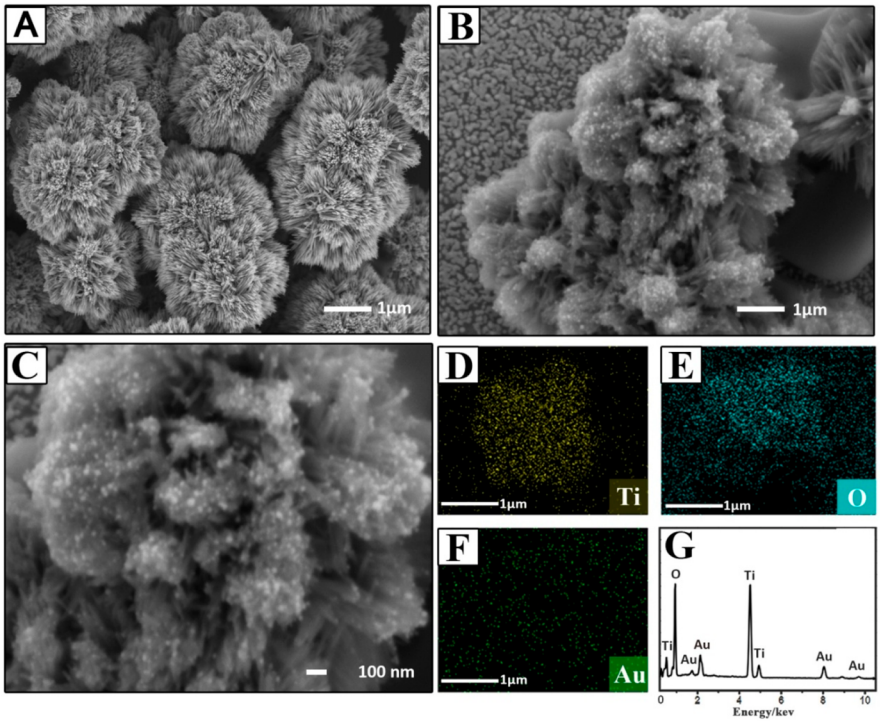

Figure 1. SEM of (A) $pTiO_2$ MSs/ITO, (B) Au NPs/$pTiO_2$ MSs/ITO, (C) a magnified view of Au NPS/$pTiO_2$ MSs. SEM-EDX elemental mapping of (D) Ti, (E) O, and (F) Au. (G) EDX spectra of Au NPs/$pTiO_2$ MSs.

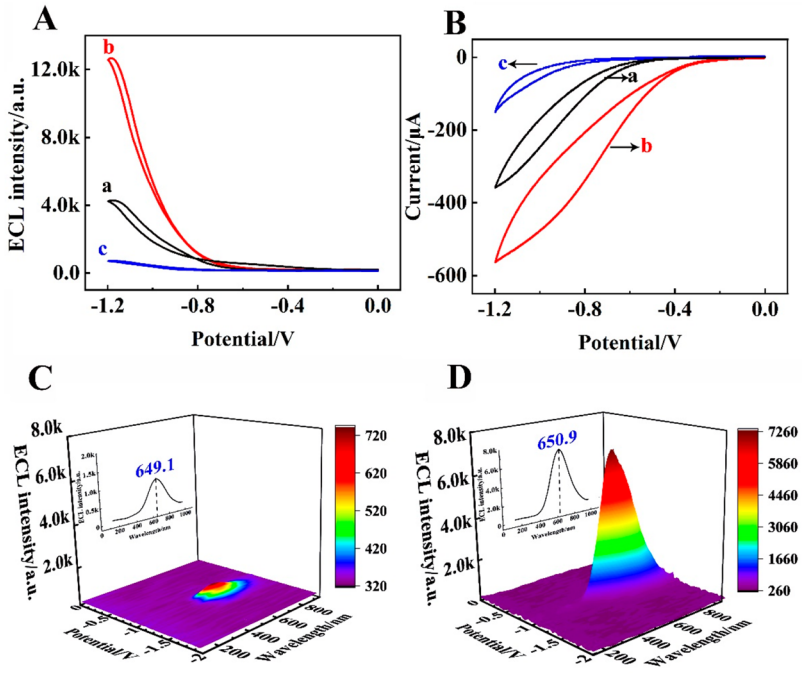

Figure 2. (A) ECL-potential curves and (B) CV of bare ITO (curve a), $pTiO_2$ MSs/ITO in PBS containing 50 mM $S_2O_8^{2-}$(curve b), $pTiO_2$ MSs/ITO in N_2-saturated PBS containing 50 mM $S_2O_8^{2-}$ (curve c). The 3D surface image model of (C) bare ITO and (D) $pTiO_2$ MSs/ITO in PBS containing 50 mM $S_2O_8^{2-}$. (Inset: the corresponding ECL-wavelength curve.)

μM), AP (4 μM), CP_2 (4 μM), and L-Fc (4 μM) was annealed for 10 min at 95 °C, then quickly refrigerated to 0 °C in 5 min. Prior to this treatment, all DNA oligonucleotide probes were prepared to the final concentration of 4 μM with hybridization buffer (HB) containing 12.5 mM Mg^{2+}.

Fabrication and Detection Process of the ECL Biosensor. To achieve a clean surface of the ITO (Resistance, 8Ω), it was preprocessed by ultrasonic treatment in 10 mL deionized water, 10 mL ethanol, and 10 mL acetone in turn.[22] The bare ITO was then covered with 10 μL of $pTiO_2$ MSs (1 mg/mL) and allowed to dry at 37 °C to gain a homogeneous layer ($pTiO_2$ MSs/ITO). Afterward, to acquire the Au nanoparticles (Au NPs) modified interface (Au NPs/$pTiO_2$ MSs/ITO), the $pTiO_2$ MSs/ITO was electrostatically deposited for 10 s in a 2 mL hydrogen tetrachloroaurate hydrate

https://doi.org/10.1021/acssensors.2c01832
ACS Sens. 2022, 7, 3208−3215

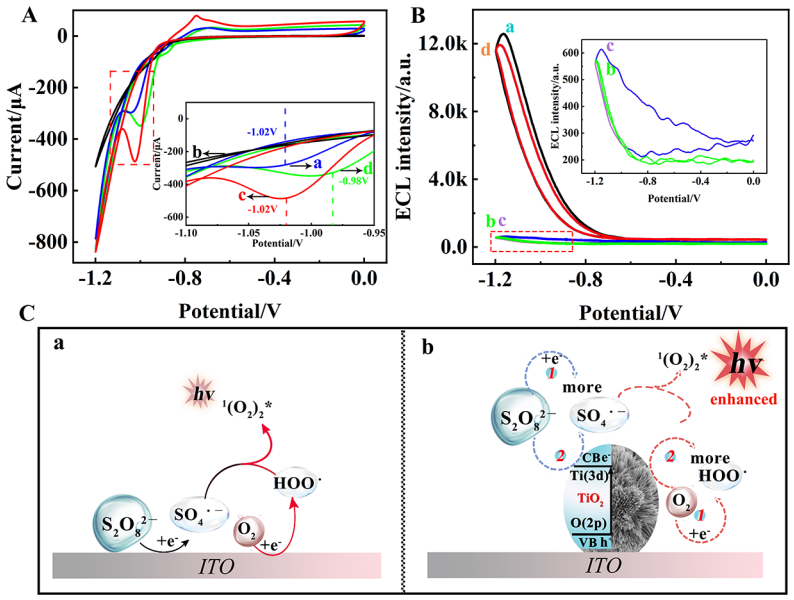

Figure 3. (A) CV of bare ITO in air-saturated PBS (curve a), N_2-saturated PBS (curve b), PBS containing 0.1 mM H_2O_2 (curve c), $pTiO_2$ MSs/ITO in air-saturated PBS (curve d). (B) ECL-times curves of $pTiO_2$ MSs/ITO in the air-saturated $S_2O_8^{2-}$ solution (curve a), $pTiO_2$ MSs/ITO in the N_2-saturated $S_2O_8^{2-}$ solution (curve b), the air-saturated $S_2O_8^{2-}$ solution containing 0.1 mM ascorbic acid (curve c), the air-saturated $S_2O_8^{2-}$ solution containing 0.1 mM isopropanol (curve d). (C) Schematic illustration of the possible ECL mechanism of (a) ITO and (b) $pTiO_2$ MSs/ITO in the air-saturated $S_2O_8^{2-}$ solution.

($HAuCl_4$, 0.01%) at −0.5 V. Following that, 10 μL Y-probes (2.5 M) were immobilized overnight at 4 °C on the surface of Au NPs/$pTiO_2$ MSs/ITO (Y-probes/Au NPs/$pTiO_2$ MSs/ITO). Then, 10 μL of hexanethiol (HT, 1 mM) was dropped on the aforementioned ITO for 40 min to block the nonspecific recognition sites. The electrodes were washed with phosphate buffered saline (PBS) after each step. The constructed ECL biosensor was performed in 2 mL test solution of PBS (pH 7.4) containing 50 mM $K_2S_2O_8$ with a photomultiplier tube (PMT) at 750 V and a working potential from −1.2 to 0 V.

RESULTS AND DISCUSSION

Characterizations of the Prepared $pTiO_2$ MSs and Au NPs. The morphology of the prepared $pTiO_2$ MSs was depicted through scanning electron microscopy (SEM). Figure 1A showed that the $pTiO_2$ MSs on the ITO surface had appeared as an urchin-like microstructure with an average diameter of about 2.4 μm, indicating that the $pTiO_2$ MSs possessed abundant active sites. As illustrated in Figure 1B, the Au NPs were uniformly deposited on the $pTiO_2$ MSs/ITO surface. Figure 1C was a local enlarged image of Figure 1B, which showed the Au NPs with an average diameter of about 10−13 nm. Then, to investigate the content of each element in the interface materials, SEM-energy-dispersive X-ray (SEM-EDX) mapping analysis tests were used. SEM-EDX mapping measurements of Figure 1D,E,F graphically exhibited the elemental distribution of Ti, O, and Au of the interface materials, respectively. The presence of the Au element was confirmed by EDX spectra (Figure 1G), displaying prominent peaks at 2.3 and 8.2 keV linked to the typical absorption peak of Au NPs due to the surface plasma resonance (SPR) phenomenon, which demonstrated the formation of Au NPs on the surface of $pTiO_2$ MSs.[23]

ECL and Electrochemical Characterization. In order to trace the ECL luminophore in $S_2O_8^{2-}$ solution, different modified electrodes were utilized with ECL and cyclic voltammogram (CV) measurements. When bare ITO was in $S_2O_8^{2-}$ solution (Figure 2A), the ECL emission of curve *a* was about 4555 au. Additionally, curve *a* in Figure 2B displayed the cathodic current of about 356.3 μA at −1.2 V upon the bare ITO in $S_2O_8^{2-}$ solution. When $pTiO_2$ MSs were coated on an ITO electrode ($pTiO_2$ MSs/ITO), an obvious enhancement of the ECL intensity about 12,355 au could be found in the $S_2O_8^{2-}$ solution (Figure 2A, curve b), which was 2.7-fold higher in comparison with that of bare ITO. As shown in Figure 2B curve b, the corresponding cathodic current increased to −550 μA at −1.2 V, which proved that $pTiO_2$ MSs boosted the efficiency of the reduction of $S_2O_8^{2-}$. In contrast, curve c in Figure 2A exhibited a considerable ECL decrease after immersing $pTiO_2$ MSs/ITO in the N_2-saturated $S_2O_8^{2-}$ solution and the corresponding cathodic current also decreased markedly (Figure 2B, curve c), which demonstrated that the ECL was dependent on DO. Furthermore, in order to understand ECL mechanisms better, 3D images of ECL obtained from different ITO could be used to track the ECL spectrum. The onset ECL spectrum was recorded at −1.2 V with the maximum ECL spectrum about 649.1 nm on bare ITO (Figure 2C) and 650.9 nm on $pTiO_2$ MSs/ITO (Figure 2D) in $S_2O_8^{2-}$ solution, which is consistent with previous reports,[24] revealing that the excited-state species was $^1(O_2)_2$*.

Possible ECL Reaction Mechanism. CV experiments were performed to study its catalytic effect on DO. As illustrated in Figure 3A, bare ITO (curve a) exhibited a reduction peak at −1.02 V in PBS. Then, the reduction peak disappeared and current density was decreased in N_2-saturated PBS (curve b). As expected, a distinct reduction peak appeared when adding H_2O_2 solution to the PBS (curve c), corroborating the generation of ROS via DO reduction at −1.02 V.[25] As observed in curve d, when $pTiO_2$ MSs were modified on ITO, the reduction peak in PBS positively shifted from −1.02 V to −0.98 V, suggesting that $pTiO_2$ MSs could catalyze the reduction reaction of DO. It was assumed that oxygen vacancies existed in TiO_2 nanoparticles could lead to

https://doi.org/10.1021/acssensors.2c01832
ACS Sens. 2022, 7, 3208−3215

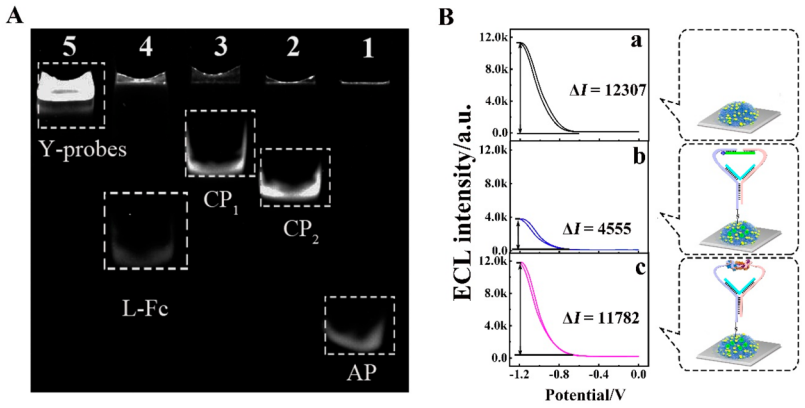

Figure 4. (A) PAGE image of the Y-probes. Lane 1: AP, Lane 2: CP_2, Lane 3: CP_1, Lane 4: L-Fc, Lane 5: the mixtures of AP, CP_1, CP_2, and L-Fc. (B) ECL responses of Au NPs/$pTiO_2$ MSs/ITO (a), Y-probes/Au NPs/$pTiO_2$ MSs/ITO (b), and cTnI/Y-probes/Au NPs/$pTiO_2$ MSs/ITO (c).

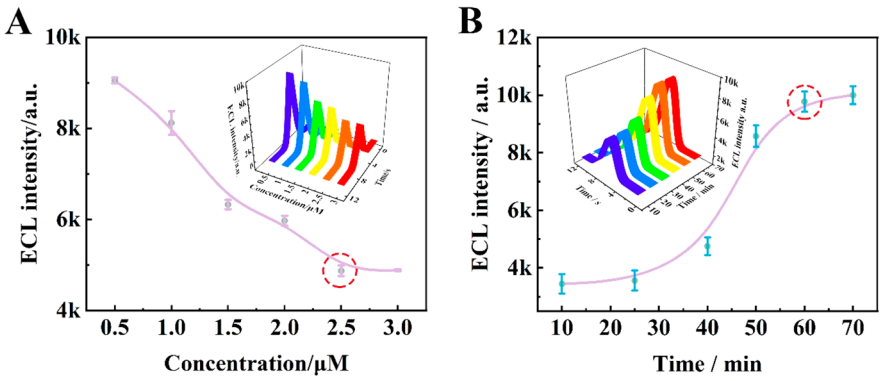

Figure 5. Optimization of the experimental conditions. (A) The concentration of Y-probes: 0.5 μM, 1 μM, 1.5 μM, 2 μM, 2.5 μM, and 3 μM. (B) The incubation time of the cTnI (1 ng mL^{-1}) toward the biosensor: 10 min, 20 min, 30 min, 40 min, 50 min, 60 min, and 70 min. Error bars: SD, n = 3.

faster electron transfer required for subsequent electrochemical conversion to produce more ROS.[26,27] To further identify the types of ROS (such as $OH^{\bullet}$, $HOO^{\bullet}$, etc.) involved in the formation of $^1(O_2)_2$*, the specific radical scavengers[28] including ascorbic acid ($HOO^{\bullet}$ radical scavenger) and isopropanol ($OH^{\bullet}$ radical scavenger) were introduced to $S_2O_8^{2-}$ solution to evaluate the ECL response. As illustrated in Figure 3B, curve a showed an obvious ECL emission of $pTiO_2$ MSs/ITO in the air-saturated $S_2O_8^{2-}$ solution. When ascorbic acid was added into the test solution, the intensity of ECL was quenched from 12,359 au to 576 au (Figure 3B, curve b), which was consistent with that in the N_2-saturated $S_2O_8^{2-}$ solution (Figure 3B, curve c), indicating $HOO^{\bullet}$ participated in the generation of $^1(O_2)_2$* directly. However, when isopropanol was added into the $S_2O_8^{2-}$ solution, the ECL response has almost no difference compared to that of $pTiO_2$ MSs/ITO (Figure 3B, curve a), signifying that $OH^{\bullet}$ had not contributed in the dominant radical pathway to generate $^1(O_2)_2$*. In summary, the enhanced ECL produced by $^1(O_2)_2$* was ascribed to a dual promoting effect of $pTiO_2$ MSs, which not only played the role of a conventional coreaction accelerator to catalyze the reduction of $S_2O_8^{2-}$, but also promoted electrochemical reaction of DO for more ROS generation. The ECL mechanism was briefly shown in Figure 3C and described in detail in the Section 6 of the SI.

Feasibility Evaluation of the Proposed Biosensor. The assembly of the Y-probes was determined by employing polyacrylamide gel electrophoresis (PAGE). The separate bands in lanes 1−4, as shown in Figure 4A, corresponded to the DNA single strands of the AP, CP_2, CP_1, and L-Fc, respectively, which had a variable electrophoresis rate toward the numbers of various bases. Particularly, in lane 5, there was a distinct bright band with the slowest migration rate, which may be attributed to the hybridization of four DNA strands to assemble the Y-probes.

The initial ECL signal measured by the Au NPs/$pTiO_2$ MSs/ITO was around 12,307 au (Figure 4B, curve a). The low ECL emission was approximately 4555 au in $S_2O_8^{2-}$ solution was obtained by Y-probes/Au NPs/$pTiO_2$ MSs/ITO, because the Fc molecule of Y-probes could quench the ECL signal (Figure 4B, curve b). An extremely high ECL recovery (about 11,782 au) was achieved when the anchored Y-probes interacted with cTnI (ng mL^{-1}), which caused the L-Fc to leave the interface, indicating the "signal-on" biosensor was successfully constructed (Figure 4B, curve c).

Optimization of the Experimental Conditions. The critical experimental parameters such as Y-probe concentration and cTnI reaction time were studied to achieve the optimal performance of the ECL biosensor. To generate a comparatively low initial signal, Y-probes with varied gradient concentrations were immobilized on Au NPs/$pTiO_2$ MSs/ITO. Figure 5A showed the impact of ECL response with different concentrations of Y-probes, where the intensity of ECL was quenched as the concentration of Y-probes increased and reached a plateau at 2.5 μM. Thus, the concentration of Y-probes was determined to be 2.5 μM. As illustrated in Figure

https://doi.org/10.1021/acssensors.2c01832
ACS Sens. 2022, 7, 3208−3215

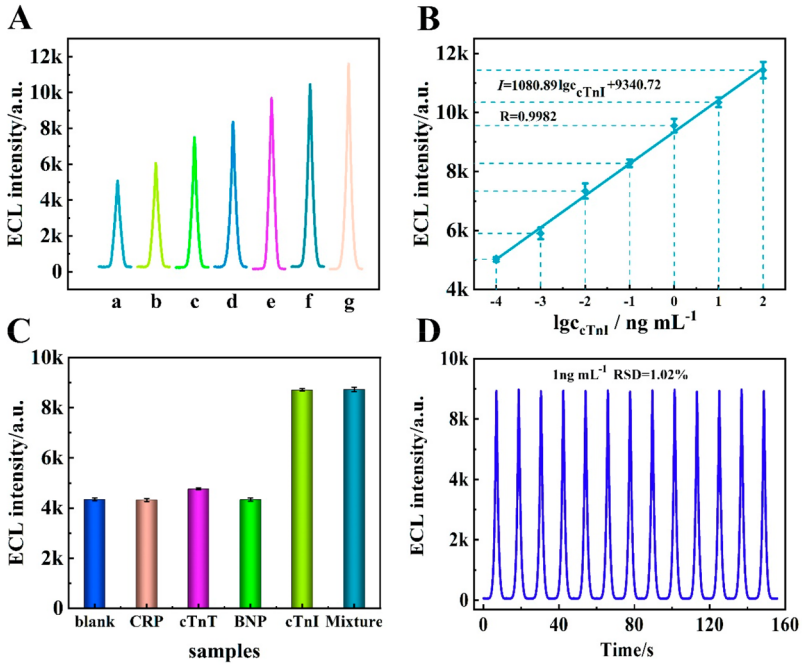

Figure 6. (A) ECL-time curves of the biosensor to different cTnI concentrations: 100 fg mL^{-1}, 1 pg mL^{-1}, 10 pg mL^{-1}, 100 pg mL^{-1}, 1 ng mL^{-1}, 10 ng mL^{-1}, and 100 ng mL^{-1} (from a−g). (B) Calibration plot of ECL intensity with logarithm of cTnI concentration. (C) The selectivity of the proposed biosensor with different interference. (D) The stability of the proposed biosensor with 1 ng mL^{-1} cTnI (Error bars: SD, n = 3).

Table 1. Performance Comparison of This Work with Other cTnI Discrimination Methods

Measurement technique	Linear range	Detection limit	Incubation time	Ref
EC	0.01 pg mL^{-1}−100 ng mL^{-1}	1.24 fg mL^{-1}	100 min	30
Fluorescent	0.12 ng mL^{-1}−125 ng mL^{-1}	0.036 ng mL^{-1}	200 min	31
ECL	0.05 pg mL^{-1}−0.1 ng mL^{-1}	0.017 pg mL^{-1}	150 min	32
Colorimetric	2 fg mL^{-1}−20 pg mL^{-1}	0.96 fg mL^{-1}	240 min	33
ECL	100 fg mL^{-1}−100 ng mL^{-1}	30.1 fg mL^{-1}	60 min	This work

5B, the ECL intensity consecutively increased along with the extension of reaction time of cTnI and trended to a plateau at 60 min, which served as the optimal reaction time of the cTnI in the work.

cTnI Discrimination Analysis. Under optimal conditions, the proposed performance of the biosensor was assessed for cTnI discrimination. The ECL responses were enhanced gradually when the cTnI concentration increased from 100 fg mL^{-1} to 100 ng mL^{-1} (Figure 6A). Usually, the concentration of cTnI in normal people ranged from 0.5 ng mL^{-1} to 2.0 ng mL^{-1}, while it would increase to 50 ng mL^{-1} in 3−6 h when AMI occurred and finally reached about 550 ng mL^{-1},[29] which could be covered in the linear range of the proposed biosensor. According to the calibration plot in Figure 6B, the ECL signal and logarithm value of cTnI concentration showed a favorable linear relationship, and the equation of linear regression was I = 1080.89 lg c + 9340.72, with an estimated limit of detection (LOD) of 30.1 fg mL^{-1}. The specific calculation process is depicted in the Section 7 of the SI.

Compared with the previous work, the cTnI biosensor developed in this work has faster detection speed and higher sensitivity, combining the advantages of proximal affinity and aptamers. The proposed biosensor in this work is time-saving besides sensitive in terms of recognition. Some interfering proteins, such as brain type natriuretic peptide (BNP), C-reactive protein (CRP), and cardiac troponin T (cTnT) were also examined to assess the selectivity of the biosensor. The three interfering proteins exhibited slight ECL increase compared to the blank experiment (no target cTnI), as shown in Figure 6C, which proved that the interference proteins had little influence on the biosensor. The mixture of CRP (1 ng mL^{-1}), cTnT (1 ng mL^{-1}), BNP (1 ng mL^{-1}), and cTnI (1 ng mL^{-1}) was examined with a notable ECL intensity, which was consistent with reaction of cTnI. Based on the findings, the proposed biosensor displayed high selectivity in addition to sensitive detection of cTnI. Furthermore, Figure 6D showed that the ECL biosensor showed exceptional stability during continuous potential scanning for 13 cycles with 1 ng mL^{-1} cTnI, with a relative standard deviation (RSD) of 1.02%. The proposed biosensor had a comparative advantage for cTnI discrimination in comparison to the previous work, as shown in Table 1 and Section 8 in SI.

Applications of the Proposed ECL Biosensor in Human Serum. The practicality of the proposed biosensor for the discrimination of cTnI was evaluated by the standard addition method. The cTnI standard solutions were diluted with human serum to different concentrations (100 fg mL^{-1}−100 ng mL^{-1}). Then the proposed ECL biosensors were incubated with the cTnI solutions in different concentrations at 37 °C for 60 min and washed with deionized water. The test was repeated three times, and the stable ECL intensity values obtained from three consecutive ECL scans were averaged. The corresponding cTnI concentration and recovery rate could be calculated according to the cTnI standard curve (Figure

https://doi.org/10.1021/acssensors.2c01832
ACS Sens. 2022, 7, 3208−3215

6B). The recovery of cTnI was in the range of 91.2% to 117%, as indicated in Table 2. Furthermore, the results of cTnI

Table 2. Applications of the Biosensor under Different Concentrations of cTnI Solution Diluted with Human Serum

Sample label	Added concentration (ng L^{-1})	Measured concentration (ng L^{-1})	Recovery (%)
1	1.00×10^{-4}	1.10×10^{-4}	110
2	1.00×10^{-3}	0.974×10^{-3}	97.4
3	1.00×10^{-2}	0.912×10^{-2}	91.2
4	1.00×10^{-1}	1.06×10^{-1}	106
5	1.00	0.977	97.7
6	10.0	11.6	116
7	100	117	117

detected by the developed biosensors were also highly consistent with that of commercialized cTnI ELISA kits obtained from zybio Inc. (Section 9 in SI). Thus, the proposed biosensor appears to be a viable device for cTnI discrimination in actual samples.

CONCLUSIONS

In summary, an exogenous luminophore-free and disposable ECL biosensor was developed and further combined with the highly specific Y-probes as a bivalent recognition element to achieve the sensitive and rapid detection of cTnI. The $pTiO_2$ MSs with huge surface area and cavity structure demonstrated a dual promoting effect for ECL amplification, because $pTiO_2$ MSs not only catalyzed DO to produce ROS, but also improved the reduction reaction of $S_2O_8^{2-}$ for $SO_4^{\bullet-}$ generation. Moreover, thanks to the bivalent aptamer structure, the Y-probes demonstrated significantly enhanced recognition specificity and efficiency toward cTnI. Such a proposed ECL biosensor points to a new avenue for the biomarker discrimination, which can also be ingeniously expanded as a portable home tester for the development of ECL biosensors in practical applications.

ASSOCIATED CONTENT

Supporting Information

The Supporting Information is available free of charge at https://pubs.acs.org/doi/10.1021/acssensors.2c01832.

Reagents, materials and apparatus used in this work, fabrication of biosensor, ECL measurement procedure, gel electrophoresis, possible ECL mechanism of DO in $S_2O_8^{2-}$ solution, the specific calculation process of LOD, comparison of the optimized response time, and comparison of the results with commercialized cTnI ELISA kit (PDF)

AUTHOR INFORMATION

Corresponding Author

Ying Zhuo − *Key Laboratory of Luminescence Analysis and Molecular Sensing (Southwest University), Ministry of Education, College of Chemistry and Chemical Engineering, Southwest University, Chongqing 400715, P. R. China;* orcid.org/0000-0002-4491-1186; Phone: +86 23 68253172; Email: yingzhuo@swu.edu.cn

Authors

Xian-Ming Guo − *Key Laboratory of Luminescence Analysis and Molecular Sensing (Southwest University), Ministry of Education, College of Chemistry and Chemical Engineering, Southwest University, Chongqing 400715, P. R. China*

Mei-Ling Zhao − *Key Laboratory of Luminescence Analysis and Molecular Sensing (Southwest University), Ministry of Education, College of Chemistry and Chemical Engineering, Southwest University, Chongqing 400715, P. R. China*

Wen-Bin Liang − *Key Laboratory of Luminescence Analysis and Molecular Sensing (Southwest University), Ministry of Education, College of Chemistry and Chemical Engineering, Southwest University, Chongqing 400715, P. R. China*

Xia Yang − *Key Laboratory of Luminescence Analysis and Molecular Sensing (Southwest University), Ministry of Education, College of Chemistry and Chemical Engineering, Southwest University, Chongqing 400715, P. R. China;* orcid.org/0000-0003-0897-2106

Ruo Yuan − *Key Laboratory of Luminescence Analysis and Molecular Sensing (Southwest University), Ministry of Education, College of Chemistry and Chemical Engineering, Southwest University, Chongqing 400715, P. R. China;* orcid.org/0000-0003-3664-6236

Complete contact information is available at: https://pubs.acs.org/10.1021/acssensors.2c01832

Notes

The authors declare no competing financial interest.

ACKNOWLEDGMENTS

This work was financially supported by the NNSF of China (22022408), the Chongqing Talents Support Program (CQYC201905067), and the Fundamental Research Funds for the Central Universities (XDJK2019TJ002), China.

REFERENCES

(1) Park, K. C.; Gaze, D. C.; Collinson, P. O.; Marber, M. S. Cardiac troponins: from myocardial infarction to chronic disease. *Cardiovasc. Res.* **2017**, *113*, 1708−1718.

(2) Liu, A.; Anfossi, L.; Shen, L.; Li, C.; Wang, X. Non-competitive immunoassay for low-molecular-weight contaminant detection in food, feed and agricultural products: A mini-review. *Trends. Food Sci. Technol.* **2018**, *71*, 181−187.

(3) Hasegawa, H.; Savory, N.; Abe, K.; Ikebukuro, K. Methods for improving aptamer binding affinity. *Molecules* **2016**, *21*, 421.

(4) Zhang, H.; Li, F.; Dever, B.; Wang, C.; Li, X. F.; Le, X. C. Assembling DNA through affinity binding to achieve ultrasensitive protein detection. *Angew. Chem., Int. Ed. Engl.* **2013**, *52*, 10698−10705.

(5) Zhao, M. L.; Zeng, W. J.; Chai, Y. Q.; Yuan, R.; Zhuo, Y. An affinity-enhanced DNA intercalator with intense ECL embedded in DNA hydrogel for biosensing applications. *Anal. Chem.* **2020**, *92*, 11044−11052.

(6) Yang, S. S.; Jiang, M. H.; Chai, Y. Q.; Yuan, R.; Zhuo, Y. Application of antibody-powered triplex-DNA nanomachine to electrochemiluminescence biosensor for the detection of anti-digoxigenin with improved sensitivity versus cycling strand displacement reaction. *ACS Appl. Mater. Interfaces.* **2018**, *10*, 38648−38655.

(7) Shen, B.; Wu, Q.; Fan, Y.; Wu, H.; Li, X.; Zhao, X.; Wang, Y.; Ding, S.; Zhang, J. TiO_2@Ag nanozyme enhanced electrochemiluminescent biosensor coupled with DNA nanoframework-carried emitters and enzyme-assisted target recycling amplification for ultrasensitive detection of microRNA. *Chem. Eng. J.* **2022**, *445*, 136820 DOI: 10.1016/j.cej.2022.136820.

(8) Chai, D. D.; Zhuo, Y.; Tu, T. T.; Li, H. L.; Yuan, R.; Wei, S. P. Ag@Pyc nanocapsules as electrochemiluminescence emitters for an ultrasensitive assay of the APE1 activity. *Anal. Chem.* **2022**, *94*, 9934−9939.
(9) Liao, N.; Zhong, X.; Liang, W. B.; Yuan, R.; Zhuo, Y. Metal-organic Frameworks (MOF)-based Novel Electrochemiluminescence Biosensing Platform for Quantification of H_2O_2 Releasing from Tumor Cells. *Acta Chim. Sinica* **2021**, *79*, 1257−1264.
(10) Wang, P.; Liang, Z.; Zhao, J.; Nie, Y.; Xu, S.; Ma, Q. A polarization-resolved ECL strategy based on the surface plasmon coupling effect of orientational Au nanobipyramids patterned structures. *Chem.Eng. J.* **2022**, *448*, 137630.
(11) Bahari, D.; Babamiri, B.; Moradi, K.; Salimi, A.; Hallaj, R. Graphdiyne nanosheet as a novel sensing platform for self-enhanced electrochemiluminescence of MOF enriched ruthenium (II) in the presence of dual co-reactants for detection of tumor marker. *Biosens. Bioelectron.* **2022**, *195*, 113657.
(12) Liao, N.; Pan, M. C.; Chen, J. F.; Zhong, X.; Yuan, R.; Zhuo, Y. A dual engine-triggered DNA walker based on luminous perylene-TiO_2 nanospheres for efficient electrochemiluminescence bioassay. *Chem. Eng. J.* **2022**, *450*, 138284 DOI: 10.1016/j.cej.2022.138284.
(13) Zhong, X.; Yang, S. S.; Liao, N.; Yuan, R.; Zhuo, Y. Development of hollow electrochemiluminescent nanocubes combined with a multisite-anchored DNA nanomachine for mycotoxin detection. *Anal. Chem.* **2021**, *93*, 5301−5308.
(14) Zhao, M.; Chen, A. Y.; Huang, D.; Chai, Y. Q.; Zhuo, Y.; Yuan, R. MoS_2 quantum dots as new electrochemiluminescence emitters for ultrasensitive bioanalysis of lipopolysaccharide. *Anal. Chem.* **2017**, *89*, 8335−8342.
(15) Tao, X. L.; Pan, M. C.; Yang, X.; Yuan, R.; Zhuo, Y. CDs assembled metal-organic framework: Exogenous coreactant-free biosensing platform with pore confinement-enhanced electrochemiluminescence. *Chin. Chem. Lett.* **2022**, *33*, 4803−4807.
(16) Jiang, D.; Wei, M.; Du, X.; Qin, M.; Shan, X.; Chen, Z. One-pot synthesis of ZnO quantum dots/N-doped Ti3C2MXene: Tunable nitrogen-doping properties and efficient electrochemiluminescence sensing. *Chem. Eng. J.* **2022**, *430*, 132771.
(17) Pan, M. C.; Lei, Y. M.; Chai, Y. Q.; Yuan, R.; Zhuo, Y. In situ controllable generation of copper nanoclusters confined in a poly-l-cysteine porous film with enhanced electrochemiluminescence for alkaline phosphatase detection. *Anal. Chem.* **2020**, *92*, 13581−13587.
(18) Tu, T. T.; Lei, Y. M.; Chai, Y. Q.; Zhuo, Y.; Yuan, R. Organic dots embedded in mesostructured silica xerogel as high-performance ECL emitters: Preparation and application for microRNA-126 detection. *ACS Appl. Mater. Interfaces.* **2020**, *12*, 3945−3952.
(19) Ma, J.; Wang, W.; Li, Y.; Lu, Z.; Tan, X.; Han, H. Novel porphyrin Zr metal-organic framework (PCN-224)-based ultrastable electrochemiluminescence system for PEDV sensing. *Anal. Ch em.* **2021**, *93*, 2090−2096.
(20) Zhou, Y.; Wang, H.; Zhuo, Y.; Chai, Y.; Yuan, R. Highly efficient electrochemiluminescent silver nanoclusters/titanium oxide nanomaterials as a signal probe for ferrocene-driven light switch bioanalysis. *Anal. Chem.* **2017**, *89*, 3732−3738.
(21) Sun, Z.; Kim, J. H.; Zhao, Y.; Bijarbooneh, F.; Malgras, V.; Lee, Y.; Kang, Y. M.; Dou, S. X. Rational design of 3D dendritic TiO_2 nanostructures with favorable architectures. *J. Am. Chem. Soc.* **2011**, *133*, 19314−19317.
(22) Yang, X.; Wei, Y.; Wang, Z.; Wang, J.; Qi, H.; Gao, Q.; Zhang, C. Highly efficient electrogenerated chemiluminescence quenching on lipid-Coated multifunctional magnetic nanoparticles for the determination of proteases. *Anal. Chem.* **2022**, *94*, 2305−2312.
(23) Devi, T. A.; Sivaraman, R. M.; Thavamani, S. S.; Amaladhas, T. P.; AlSalhi, M. S.; Devanesan, S.; Kannan, M. M. Green synthesis of plasmonic nanoparticles using Sargassum ilicifolium and application in photocatalytic degradation of cationic dyes. *Environ. Res.* **2022**, *208*, 112642.
(24) Xiao, S. Y.; Li, Y.; Zhen, S. J.; Huang, C. Z.; Li, Y. F. Efficient peroxydisulfate electrochemiluminescence system based the novel silver metal-organic gel as an effective enhancer. *Electrochim. Acta* **2020**, *357*, 136842.
(25) Schurmann, A.; Luerssen, B.; Mollenhauer, D.; Janek, J.; Schroder, D. Singlet oxygen in electrochemical cells: A critical review of literature and theory. *Chem. Rev.* **2021**, *121*, 12445−12464.
(26) Li, Y. F.; Selloni, A. Theoretical study of interfacial electron transfer from reduced anatase $TiO_2(101)$ to adsorbed O_2. *J. Am. Chem. Soc.* **2013**, *135*, 9195−9199.
(27) Nosaka, Y.; Nosaka, A. Y. Generation and detection of reactive oxygen species in photocatalysis. *Chem. Rev.* **2017**, *117*, 11302−11336.
(28) Cui, W. R.; Li, Y. J.; Jiang, Q. Q.; Wu, Q.; Luo, Q. X.; Zhang, L.; Liang, R. P.; Qiu, J. D. Covalent organic frameworks as advanced uranyl electrochemiluminescence monitoring platforms. *Anal. Chem.* **2021**, *93*, 16149−16157.
(29) Han, X.; Li, S. H.; Peng, Z. L.; Othman, A. M.; Leblanc, R. Recent Development of Cardiac Troponin I Detection. *ACS Sens.* **2016**, *1*, 106−114.
(30) Chen, K.; Zhao, H.; Wang, Z.; Zhou, F.; Shi, Z.; Cao, S.; Lan, M. Sandwich-type electrochemical aptasensor based on Au-modified conductive octahedral carbon architecture and snowflake-like PtCuNi for the sensitive detection of cardiac troponin I. *Biosens. Bioelectron.* **2022**, *212*, 114431.
(31) Song, S. Y.; Han, Y. D.; Kim, K.; Yang, S. S.; Yoon, H. C. A fluoro-microbead guiding chip for simple and quantifiable immunoassay of cardiac troponin I (cTnI). *Biosens. Bioelectron.* **2011**, *26*, 3818−3824.
(32) Hong, C.; Zhang, P.; Lu, K.; Ji, Y.; He, S.; Liu, D.; Jia, N. A dual-signal electrochemiluminescence immunosensor for high-sensitivity detection of acute myocardial infarction biomarker. *Biosens. Bioelectron.* **2021**, *194*, 113591.
(33) Mi, X.; Li, H.; Tan, R.; Feng, B.; Tu, Y. The TDs/aptamer cTnI biosensors based on HCR and Au/Ti_3C_2-MXene amplification for screening serious patient in COVID-19 pandemic. *Biosens. Bioelectron.* **2021**, *192*, 113482.